

Boost the Performance of Triboelectric Nanogenerators through Circuit Oscillation

Sixing Xu, Wenbo Ding, Hengyu Guo, Xiaohong Wang,* and Zhong Lin Wang*

Triboelectric nanogenerator (TENG) which harvests ubiquitous ambient mechanical energy is a promising power source that can meet the distributed energy demand in the internet of things, wearable electronics, etc. However, the available output of TENG is severely limited by the saturated polarized charge density, small intrinsic capacitance, and large matching impedance. Herein, an effective power management strategy is proposed that flips the free charges on the conductive layer through a controlled LC oscillating circuit composed of the diode, switch, inductor, and the intrinsic capacitor of TENG. In this way, the equivalent charge density reaches a level higher than the saturated polarized charge density. The simulation and experiments show that the limit of energy output can be exceeded under arbitrary load resistance, especially for the low-impedance common electronics. It is believed that such a general, low-cost, and highly effective strategy can further broaden the applications of TENG devices across the fields and probably be a new performance evaluation standard for TENG.

and sustainable energy. Triboelectric nanogenerator (TENG), as a novel mechanical energy harvesting technique invented by Wang et al., has proven to be an effective power alternative for small electronics and attracted plenty of interests in recent years.^[4–11] To make TENG more practical and compatible to the commercial electronics, it is always desirable to improve the output performance. One way is from the device perspective, for example, choosing appropriate materials, designing the device structure, etc.,^[12–21] which is effective but needs specific optimization. The other one is from the power management perspective,^[22–31] which is more general.

Over the past few years, extensive efforts have been put into the power management of TENG for enhancing its output performance.^[22–32] Zi et al.

1. Introduction

With the advancement of Internet of things (IoT) and wearable electronics, the ubiquitous sensors have brought great convenience to people's daily life but also raised huge challenges on the maintenance due to the lack of power.^[1–3] The distributed characteristics of the IoT and other commercial electronics have made necessary reliable sources of distributed

first proposed the concepts of “figure of merits” and “cycles for maximum energy output (CMEO),”^[28] which provide the guideline for the maximum energy output per cycle of a TENG device. Afterward, Xi et al.^[29] and Cheng et al.^[30] have separately demonstrated the power management circuits which assist the TENG to achieve the 72% and 80% of the CMEO. However, the further approaching or even beyond the CMEO is more than difficult. Moreover, the maximum energy output can only be achieved when the load matches the impedance of TENG. Considering the low intrinsic capacitance of TENG and low frequency characteristics of the ambient vibration, the matching impedance is always beyond magnitude of tens or hundreds of megaohms.^[15,33,34] Although several existing power management strategies can help reduce the matched impedance to several megaohms,^[28,30] it is still much larger than the input resistance of common electronics, which are typically around hundreds of ohms. Recently, Qin et al. reported an interesting TENG system which can eliminate the requirement of impedance matching,^[31] however, their system is only applicable for elaborate devices.


Herein, in both theory and experimental verification, we report a novel power management strategy named oscillation assisting TENG (OA-TENG), which can exceed the CMEO limit of individual TENG under arbitrary load resistance. Unlike the previous power management strategies, the farther the load resistance from the matching impedance, the higher energy output per cycle can be provided from the OA-TENG, which means this strategy is especially suitable for the common electronics of low resistance. This OA-TENG is achieved by

S. Xu, Dr. W. Ding, Dr. H. Guo, Prof. Z. L. Wang
School of Materials Science and Engineering
Georgia Institute of Technology
Atlanta, GA 30332-0245, USA
E-mail: zhong.wang@mse.gatech.edu

S. Xu, Prof. X. Wang
Department of Microelectronics and Nanoelectronics
Tsinghua University
Beijing 100084, China
E-mail: wxh-ime@tsinghua.edu.cn

Dr. H. Guo, Prof. Z. L. Wang
Beijing Institute of Nanoenergy and Nanosystems
Chinese Academy of Sciences
Beijing 100083, China

Prof. Z. L. Wang
School of Nanoscience and Technology
University of Chinese Academy of Sciences
Beijing 100049, China

 The ORCID identification number(s) for the author(s) of this article can be found under <https://doi.org/10.1002/aenm.201900772>.

DOI: 10.1002/aenm.201900772

simply in-series (Mode-1) or in-parallel (Mode-2) connecting an inductor and two parallel diodes, with the switch, load, and TENG device. The inductor and the intrinsic capacitance of TENG form an oscillation circuit so that the voltage and charge of TENG will flip and accumulate in each cycle. According to the simulation, for a free-standing mode TENG with intrinsic capacitance of 0.5 nF, open-circuit voltage of 100 V, and harmonic excitation frequency of 1 Hz, the output of OA-TENG is improved by 6 orders for load resistance of 1 kΩ and the minimum of 3 times at the impedance of 1 GΩ, compared with the CMEO of individual TENG. Furthermore, a mechanical switching system is constructed for the experimental verification, in which obviously higher energy output can be observed compared with CMEO. Nonideal factors in the system are also discussed and the perspective of future improvement is proposed. The proposed scheme could broaden the potential applications of TENG in the field of IoT and wearable electronics as an effective power source.

2. Results

2.1. Mechanism and Simulation of OA-TENG

The CMEO is commonly regarded as the upper bound of the energy output per cycle of TENG.^[28,30–32] However, the physical essence behind the CMEO limit is not clear enough and the possibility to go beyond that limit is still debatable. In order to analyze this problem more intuitively, a contact-separation mode TENG is taken as an instance. **Figure 1a** shows the charge distribution of the common operation of “cycles for energy

output (CEO),” in which the polarized charge on the insulating layer is partially neutralized by the opposite charge on the adhered conductive layer, which makes the electric field energy converted from the mechanical force relatively low. Although the operation of CMEO reported by Zi et al. skillfully transfers all of that electric field energy to the load,^[32] the amount of the electric field energy keeps the same as that of CEO. The improved CMEO strategy which disconnects the TENG during the mechanical displacement so that the polarized charge will not be neutralized,^[28,30] as illustrated in **Figure 1b**. In this strategy, all of the polarized charges can be utilized and the limit of CMEO can be achieved. Hence, it can be concluded that the limit of CMEO, from a physical perspective, is actually the total electrical field energy of the polarized charges. Therefore, to break through that limit, a unique charge distribution is achieved through the LC oscillating circuit. Different from the previous work which uses resonance as signal processing,^[35] the oscillation circuit in this work flips the free charges on the conductive layer so that it will not neutralize the polarized charges, but increase the amount of equivalent charges. As shown in **Figure 1c**, the amount of the energy in the OA-TENG system increases and the limit of CMEO is easily broken through. **Figure 1d** shows a typical *V–Q* plot of the operations of CEO, CMEO, maximized CMEO, and OA-TENG, which clearly demonstrate the advantage of the OA-TENG.

The strategy of OA-TENG can be implemented by using two types of external circuits according to the load resistance. As shown in **Figure 2a**, the Mode-1 OA-TENG consists of a TENG, an external inductor, two parallel diodes, and a switch in series connection. The switch is only triggered at the positive and negative maximum points of the mechanical displacement of the

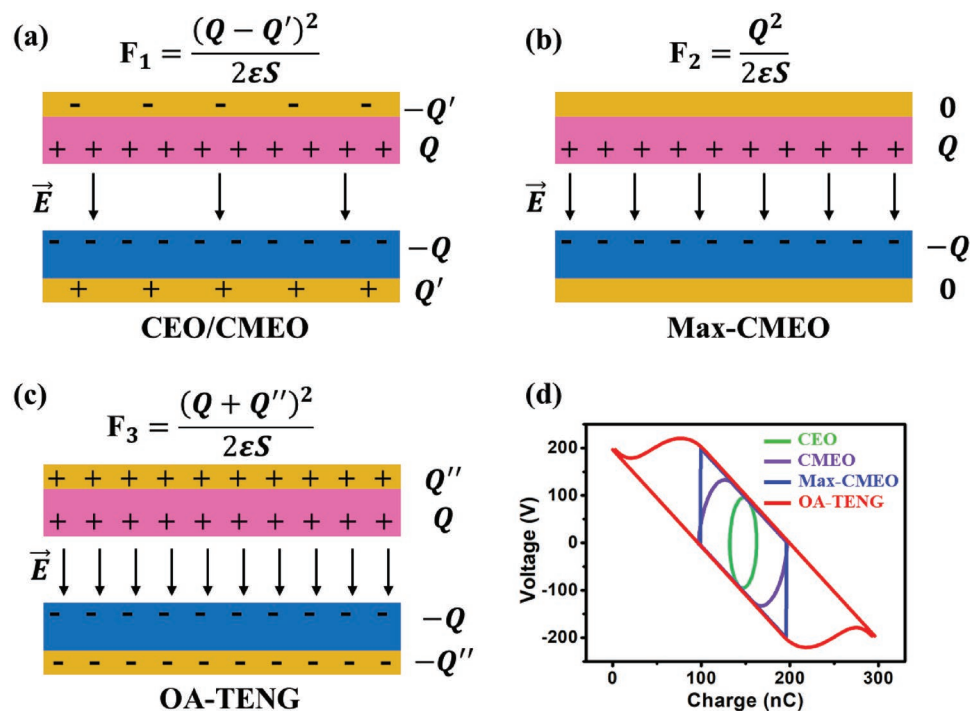


Figure 1. Comparison of operation of CEO, CMEO, Max-CMEO, and OA-TENG. The charge distribution and electrical field force of a) CEO/CMEO, b) maximized CMEO, and c) OA-TENG. d) The comparison of CEO, CMEO, maximized CMEO, and OA-TENG in *V–Q* plot.

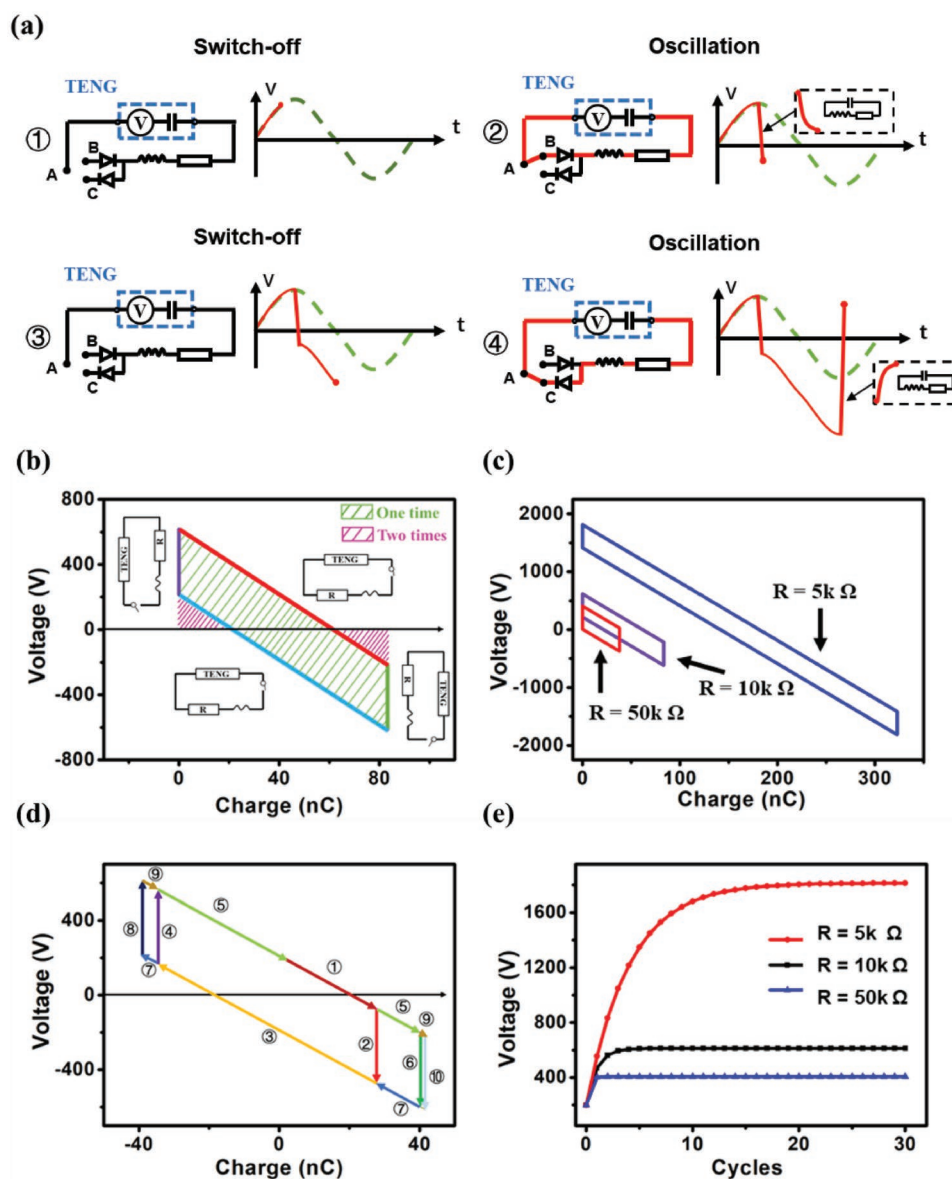


Figure 2. Mechanism and simulations of the Mode-1 OA-TENG. a) The operation cycles for Mode-1 OA-TENG. b) The V - Q curve for the steady state. c) The V - Q curves with different load resistance. d) The first several periods to achieve steady. e) The numbers of periods to achieve steady with different load resistance.

TENG. During most of the time, the switch is turned off so that the TENG is open circuit and the transferred charge is zero. When the TENG reaches the positive extreme displacement, the switch connects the terminal A and B, so that an oscillating electrical circuit composed by the intrinsic capacitor of TENG, the external inductor, and the load is established. The TENG will not only lose all of the original charges, but also reverses charges due to the oscillation until the current being cutoff by the diode. The intrinsic capacitance of the TENG is so small that the period of the oscillation is almost negligible compared with the mechanical movement.^[36] Afterward, the switch is turned off again and the TENG continues to reverse charges on the basis of the previous flipped voltage. Obviously, the absolute value of the output voltage increases compared to original

TENG (green dot line). When the TENG reaches the negative extreme point, similarly, the switch connects the terminals of A and C, and the voltage flips again. With each flip, the voltage and the charge increases, until the system saturates.

To quantitatively understand the electrical phenomenon of this system, we consider a harmonic excitation (corresponds to a single frequency in the frequency domain) for the system so that the state equation of the oscillating circuit can be written as Equation (1),^[33] where L is the inductance, R is the load resistance, C is the intrinsic capacitance of the TENG, Q is the charge of the intrinsic capacitor, ω is the angular frequency of the mechanical excitation, and V_0 is the maximum open-circuit voltage of TENG. For the analytic solution and simplicity, we consider the free-standing mode TENG here, of which the

capacitance remains constant during the movement.^[37] But it should be emphasized that the strategy is suitable for all types of TENG devices because of the same equivalent circuit model.^[35] The solution of Equation (1) is expressed in Equation (2), where the Q_1 and Q_2 are constants determined by the initial state, i.e., the condition at the beginning of the oscillation. The voltage output and transferred charges of the TENG can be easily calculated, as shown in Note S1 in the Supporting Information

$$L \frac{d^2 Q}{dt^2} + R \frac{dQ}{dt} = -\frac{Q}{C} + V_0 \cos(\omega t) \quad (1)$$

$$Q = e^{-\frac{R}{2L}t} \left[Q_1 \sin\left(\sqrt{\frac{1}{LC} - \frac{R^2}{4L^2}}t\right) + Q_2 \cos\left(\sqrt{\frac{1}{LC} - \frac{R^2}{4L^2}}t\right) \right] + \frac{C}{1 + \omega^2 R^2 C^2} V_0 \cos(\omega t) + \frac{\omega RC^2}{1 + \omega^2 R^2 C^2} V_0 \sin(\omega t) \quad (2)$$

A stable operation cycle is simulated using MATLAB with parameters listed in Table 1 and the V - Q plot is shown in Figure 2b. During the switch-off process, the output current is zero so that the process corresponds to a vertical line in the V - Q plot. While for the oscillation process, the voltage flips with a certain degree of loss due to the damping. The oscillation process is much faster than the external excitation so it corresponds to a straight line in the V - Q plot as the built-in potential of TENG is almost unchanged.

Different from the operation of CMEO which requires a large load resistance,^[32] the Mode-1 OA-TENG outputs larger energy per cycle with lower load resistance. It can be observed that Equation (2) contains two parts: the pure sinusoidal part and the damped oscillation part. When the load resistance is larger than the critical resistance as expressed in Equation (3), the circuit will not oscillate and the V - Q curve degenerates to the shape of CMEO, as illustrated in the simulation at Figure 1c. When decreasing the load resistance, the circle of the V - Q curve grows, which means more transferred charge per cycle and higher output voltage

$$R > \sqrt{\frac{4L}{C}} \quad (3)$$

It always takes several periods for the operation of the OA-TENG to reach its steady state. As shown in the simulation of Figure 1e, through each oscillation process, the charge and voltage increase and gradually saturate to the steady state. The stable condition is easy to get: the voltage loss during each oscillation is compensated by the voltage gain during the switch-off process, which can be mathematically written as Equation (4). The number of periods to reach the steady state for different load resistances is plotted in Figure 1e. It can be observed that the larger load resistance causes more voltage loss during the

Table 1. Parameters used for simulating the OA-TENG.

Open-circuit voltage	Intrinsic capacitance	External inductance	Excitation frequency	Load resistance
100 V	0.5 nF	0.5 H	1 Hz	20 kΩ

oscillation process hence the stable voltage is lower and the time to reach stable is shorter.

$$V_{\text{loss-osci}} = V_{\text{gain-switchoff}} = 2V_0 \quad (4)$$

Despite that, Mode-1 OA-TENG can achieve higher energy output per cycle with small load; its output will be reduced to the level of CMEO when the load exceeds the critical resistance shown in Equation (3). The Mode-2 OA-TENG is designed for dealing with large load. As shown in Figure 3a, the Mode-2 OA-TENG contains the same components with Mode-1 OA-TENG, yet through a parallel connection. The mechanism is also similar: most of the time, the switch is off and the TENG is directly connected to the load. When the TENG reaches the positive maximum displacement, the switch connects the terminal A and B and an oscillation electrical circuit composed by the intrinsic capacitance of TENG, the external inductor is established. The oscillation circuit is ideal without damp so that the voltage can be fully reversed. After that, the switch turned off again and the TENG continues to power the load resistance with a clearly higher voltage compared to original TENG (green dot line). When the TENG reaches the negative maximum displacement, the switch connects the terminals of A and C, and the voltage flips again. With each flip, the voltage and the charge increases, until the system saturates.

Since each oscillation process is a simple undamped LC oscillation, we pay more attention to the switch-off process. The state Equation (5) has a general solution of (6), in which Q_0 is a constant decided by the condition at the end of the oscillation process. For a common “cycles for energy output (CEO)” operation, it is easy to get that Q_0 is 0 and the output is in a purely sinusoidal shape. However, for the operation of Mode-2 OA-TENG, the Q_0 cannot be eliminated and the state Equation turns to be Equation (7), where V_1 is the voltage at the end of the oscillation. It is noteworthy that V_1 is not the peak voltage due to the RC-delay. The voltage output and transferred charge of the TENG are calculated, as shown in Note S2 in the Supporting Information.

$$\frac{dQ}{dt} + \frac{Q}{RC} = \frac{V_0}{R} \cos(\omega t) \quad (5)$$

$$Q = Q_0 e^{-\frac{t}{RC}} + \frac{CV_0 [wRC \sin(\omega t) + \cos(\omega t)]}{1 + \omega^2 R^2 C^2} \quad (6)$$

$$Q_{\text{OA-TENG}} = \left(CV_1 + \frac{\omega^2 R^2 C^2}{1 + \omega^2 R^2 C^2} CV_0 \right) e^{-\frac{t}{RC}} + \frac{CV_0 [wRC \sin(\omega t) + \cos(\omega t)]}{1 + \omega^2 R^2 C^2} \quad (7)$$

In Equation (7), there exist a sinusoidal term as well as an exponential decay term, and these two terms are competing with each other. A stable operation cycle is simulated and the V - Q plot is shown in Figure 3b. It can be observed that the curves (red and blue lines) correspond to the switch-off processes decrease at first (absolute value) under the influence of the exponential term, and then dominated by the sinusoidal term and increase. Similar to the Mode-1 OA-TENG, the oscillation processes present to be straight lines on the V - Q plot.

Even if each oscillation process is ideal, the voltage amplitude of the oscillation is not the peak voltage of the TENG, yet is affected by the load. The larger the load resistance, the

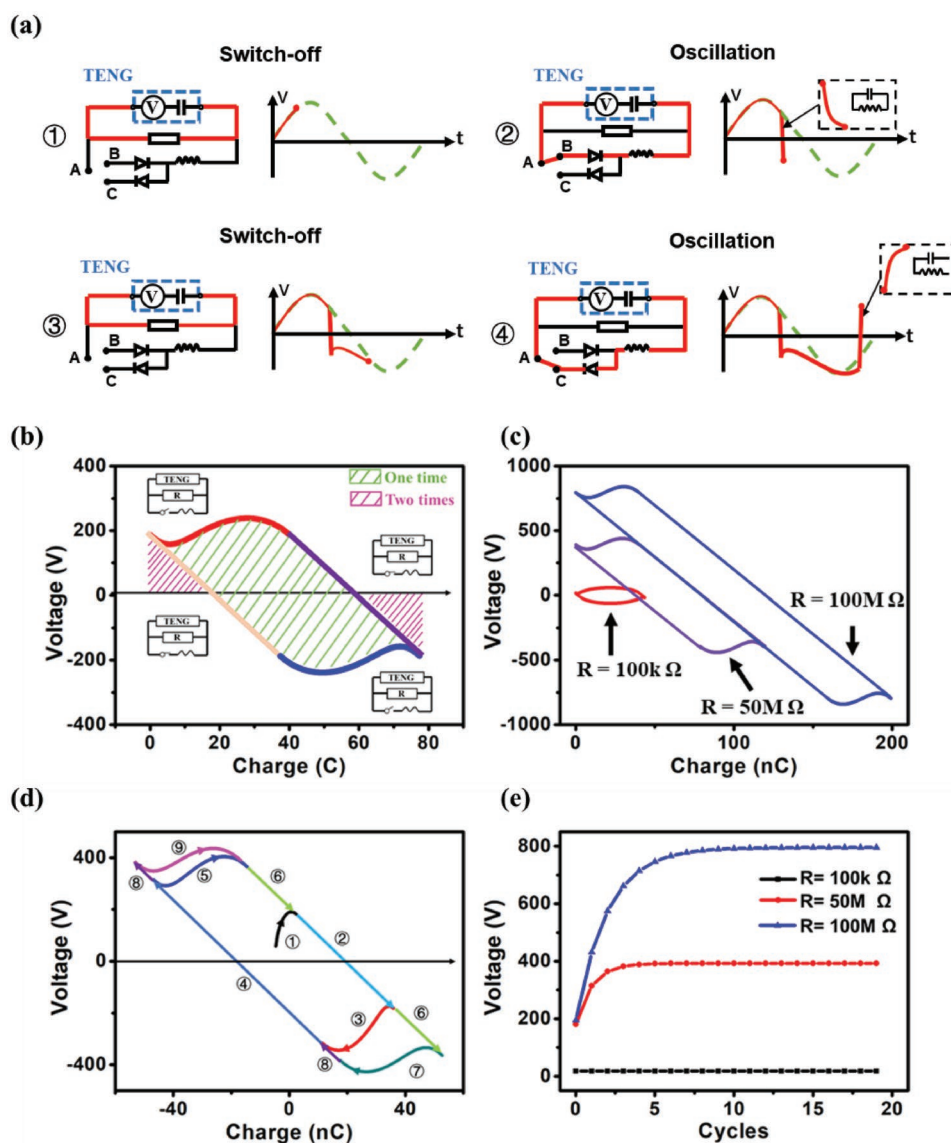


Figure 3. Mechanism and simulations of the Mode-2 OA-TENG. a) The operation cycles for Mode-2 OA-TENG. b) The V - Q curve for the steady state. c) The V - Q curves with different load resistance. d) The first several periods to achieve steady. e) The numbers of periods to achieve steady with different load resistance.

smaller RC-delay, which further brings better performance of the Mode-2 OA-TENG. The V - Q curves of Mode-2 OA-TENG with different load resistances are depicted in Figure 3c. For the small load (red cycle), the voltage drops to a very low level before it starts to oscillate and the improvement brought by the Mode-2 TENG is almost negligible. However, with the increase of the load resistance (purple and blue cycles), the oscillation becomes more obvious and the output of Mode-2 OA-TENG get higher.

Figure 3d shows the first several periods of the Mode-2 OA-TENG to get stable. It is easy to get the stable condition of the Mode-2 OA-TENG: the voltage at the beginning of the switch-off process equals to the voltage at end of the process, which mathematically can be written as Equation (8). The periods necessary to reach steady state for different load resistances

are plotted in Figure 3e. The smaller load brings a higher voltage gain of the sinusoidal term in the nonoscillatory process, which results in higher stable voltage but longer time to saturate

$$V_{\text{start-switchoff}} = V_{\text{end-switchoff}} \quad (8)$$

2.2. Experimental Demonstration of OA-TENG

Here we demonstrate that the OA-TENG can be easily achieved by combining mechanical switches with TENG devices. A free-standing mode TENG with the autoswitching device was fabricated and the parameters of the TENG are close to that in the Table 1.

First, the Mode-1 OA-TENG was demonstrated by using an external load resistance $R = 10\text{ k}\Omega$, inductance $L = 0.5\text{ H}$, and a harmonic excitation frequency of $f = 1\text{ Hz}$, as shown in Figure S1

in the Supporting Information. The voltage output of the first four periods is shown in Figure 4a. It can be observed that the voltage undergoes sharp flip at each extreme point, which

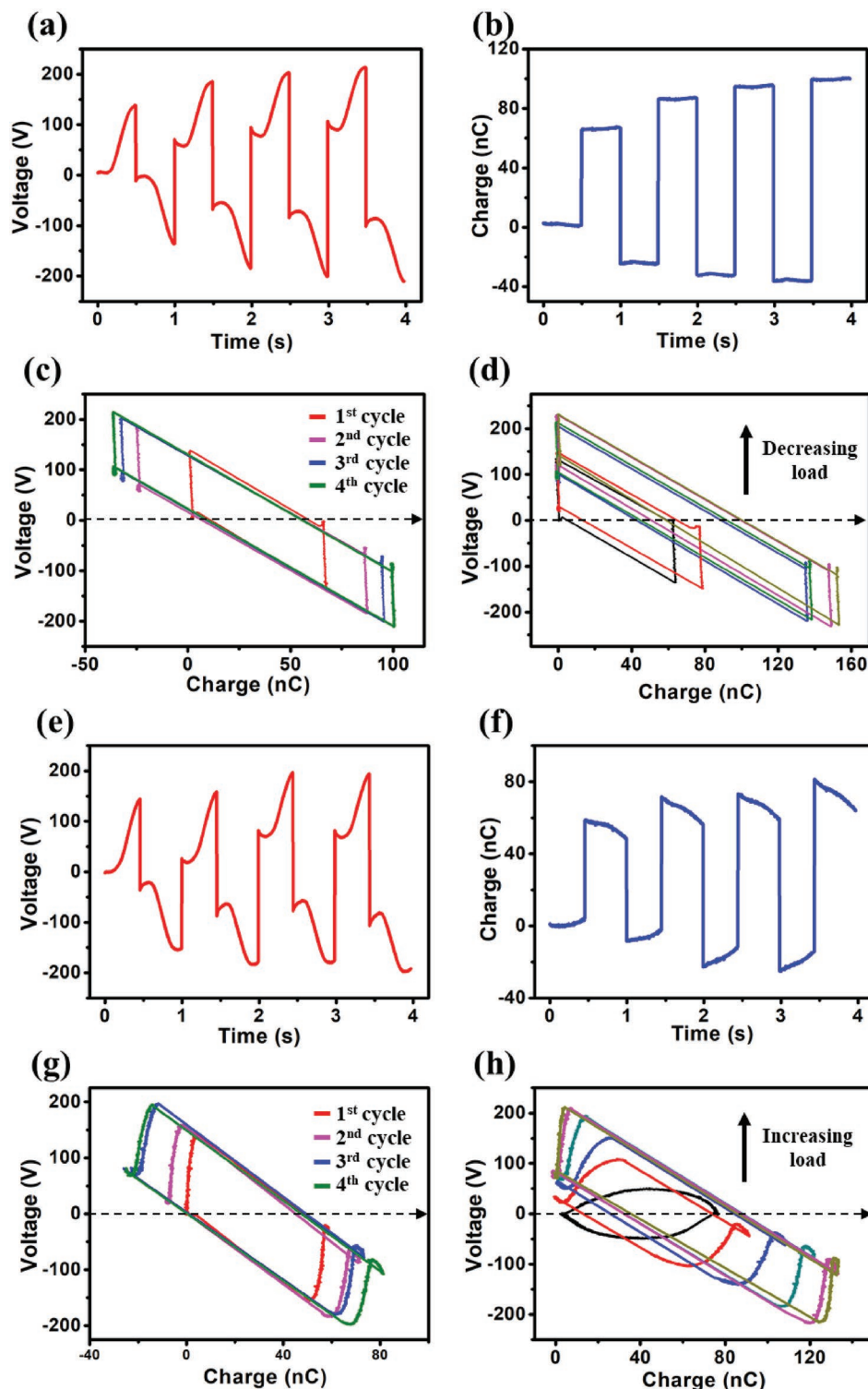


Figure 4. The experimental demonstration of OA-TENG. a) The $V-t$ curves, b) $Q-t$ curves, and c) $V-Q$ curves of the first four periods of Mode-1 OA-TENG. d) The $V-Q$ curves of Mode-1 OA-TENG with different load resistances (low to high: short circuit, $1\text{ k}\Omega$, $5\text{ k}\Omega$, $10\text{ k}\Omega$, $100\text{ k}\Omega$, $1\text{ M}\Omega$). e) The $V-t$ curves, f) $Q-t$ curves, and g) $V-Q$ curves of the first four periods of Mode-2 OA-TENG. h) The $V-Q$ curves of Mode-2 OA-TENG with different load resistances (low to high: $100\text{ M}\Omega$, $1\text{ G}\Omega$, $10\text{ G}\Omega$, $100\text{ G}\Omega$, $500\text{ G}\Omega$, open circuit).

accords with the theoretical analysis in Figure 2a and is obviously higher than the sinusoidal output of pure TENG device. The transferred charges were also measured, as illustrated in Figure 4b. The charges keep constant when the switch turns off and dramatically flip upon the establishment of the oscillating circuit. The amount of the transferred charges increases with each flip and gradually saturates. The saturation phenomenon is more obvious in the $V-Q$ plot shown in Figure 4c, which fits well with the simulation in Figure 2d. The influence of the load resistance is also investigated. As shown in Figure 4d, with a large load resistance of 10 M Ω the circuit will not oscillate due to the over-damping and the $V-Q$ curve turns into a typical curve of CMEO operation. With the decrease of the load resistance, the Mode-1 OA-TENG begins to oscillate and the amplitude of output is negatively related to the load resistance, which is the most significant difference between Mode-1 OA-TENG with CEO and CMEO.

The Mode-2 OA-TENG is also demonstrated with an external load resistance $R = 100 \text{ G}\Omega$, inductance $L = 0.5 \text{ H}$, and a harmonic excitation with frequency of $f = 1 \text{ Hz}$, as illustrated in Figure S2 in the Supporting Information. The voltage output of the first four periods is shown in Figure 4e, unlike Mode-1 OA-TENG, the voltage does not flip at the peak due to the RC-delay. It can be observed that each oscillation process does not achieve 100% voltage reversal, which is caused by the nonideal resistance in the circuit. Figure 4f illustrates the transferred charges of the first four cycles, which flow slowly during the off status of the switch but dramatically flip with the switch being turned on. The saturation phenomenon also exists at Mode-2 OA-TENG, which is clear in the $V-Q$ plot of Figure 4g. It is noteworthy that when saturated, the voltages at the beginning and the end of nonoscillatory process is not equal as predicted in Equation (8) and Figure 3d, but bring a height difference in the $V-Q$ plot. The $V-Q$ curves of the Mode-2 OA-TENG with different load resistances are shown in Figure 4h. With a small load resistance of 1 M Ω , the $V-Q$ curve turns into a typical curve of CMEO operation, which accords with the simulation shown in Figure 3c. When increase the load resistance, the Mode-2 OA-TENG begins to oscillate and the amplitude of output is positively related to the load resistance.

3. Discussion

3.1. Energy Output Per Cycle of OA-TENG

Zi et al. have proposed the method of calculating output energy per cycle for TENG.^[32] However, the calculating formula should be improved for OA-TENG. For the cycles of CMO and CMEO with pure resistive external circuit, the voltage and current should always in the same direction, so that the product of them is certainly positive. While for the inductive and capacitive external circuits, there exist phase difference between voltage and current and the reactive power is introduced. This reactive power is temporally stored in capacitors and inductors as the electromagnetic field energy, and can be further transformed into heat, light, or mechanical energy. A typical example is using electronic generators to charge a capacitor at first and then power the electronics. Therefore, based on Zi's work,^[32] we

extend the formula of energy output per cycle to calculate the apparent power, as expressed in Equation (9). Thus, the energy output of TENG is not only the enclosed area of the $V-Q$ curves, but also the coverage area of the $V-Q$ curve and the Q -axis. As demonstrated in Figures 2b and 3b, the energy output should be the sum of green area and two times of the purple area, which is clearly larger than CMO and CMEO

$$E = \bar{P} T = \int_0^T |V| dt = \int_0^T |VdQ| \quad (9)$$

The theoretical energy output per cycle of Mode-1 OA-TENG, Mode-2 OA-TENG, CEO, and CMEO with different load resistance are shown in Figure 5a. In small load and high load area, OA-TENG can achieve significantly higher energy output per cycle. By rational choosing the circuit mode, the energy output per cycle can increase at least two times for arbitrary load. We also calculated the energy output per cycle of Mode-1 and Mode-2 OA-TENG in the experimental demonstration, as shown in Figure 5b. In most of the load region, the test results show superior energy output and keep in good agreement with the theory. However, in the ultralow and ultrahigh load region, nonideal saturation appears.

3.2. Nonideal Factors

According to the theory, when the load resistance approaches zero or infinity, the output of Mode-1 OA-TENG and Mode-2 OA-TENG should reach the device breakdown limitation. However, as shown in Figure 5b, we observed the nonideal saturation below 1 k Ω and over 20 G Ω , which obviously not reach the device breakdown limitation. We believe this nonideal saturation mainly resulted from two factors: 1) the diode does not achieve the turn-on state. As shown in the $I-V$ curve of the diode (Figure S3, Supporting Information), the resistance is larger than 1 k Ω for current below 0.1 mA; 2) the time constant of the oscillating circuit is too short that the capacitor has fully discharged when the mechanical switch is not in perfect contact and an extra contact resistance is introduced. The damping caused by the diode resistance and contact resistance, on the one hand, makes the circuit unable to oscillate perfectly and results in the saturation in low load and high load areas; on the other hand, the uncontrolled resistances make the oscillation amplitude not stable. When the resistance larger than the critical resistance occasionally, the circuit will be overdamped and the system will be reset. In our future work, the system is to be improved by substituting the current nonideal components: firstly, the diode can be replaced by the active rectification circuit which relies on the metal-oxide-semiconductor field-effect transistor (MOSFET) and brings an ultralow resistance and low-power-consumption; also, the mechanical switch can be replaced by electronic switch with a peak detection circuit. For example, a low-cost voltage comparator and a simple RC delay circuit can be applied, in which the RC delay circuit provides a phase difference of the TENG output for the comparator to find the peak of the signal.

Despite these nonideal factors in current system, on average, the OA-TENG can still significantly improve the output of TENG. Figure 5c shows the long-term output of CEO, CMEO,

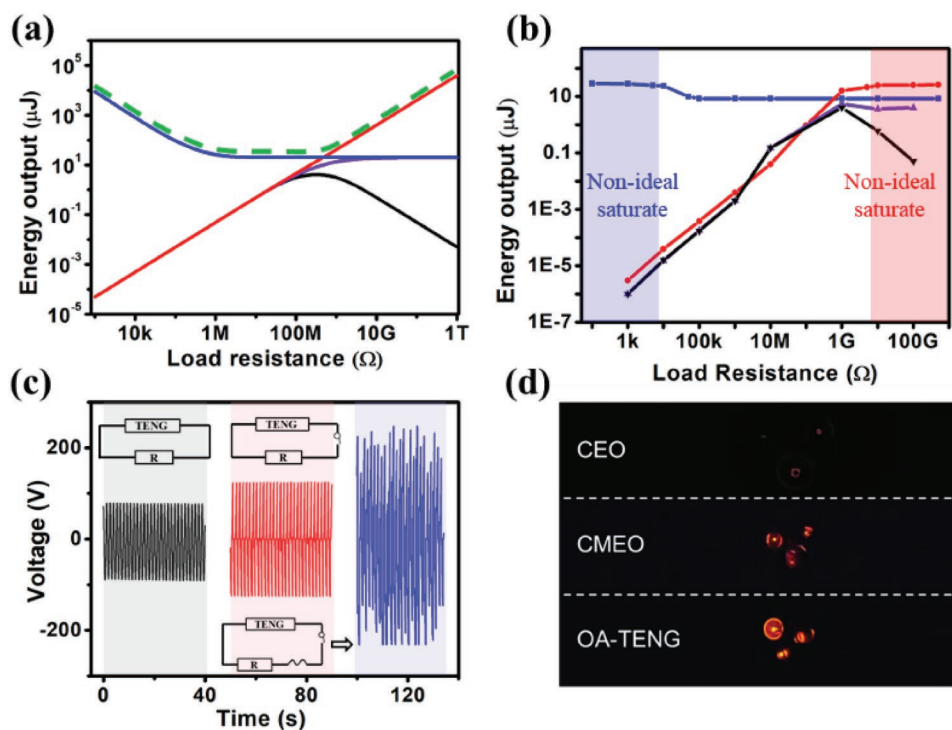


Figure 5. The energy output and nonideal factors of OA-TENG. a) The simulated energy output per cycle of Mode-1/Mode-2 OA-TENG (blue/red), CEO (black) and CMEO (purple). The overall optimized energy output of OA-TENG is plotted as green dot line, CEO (black) and CMEO (purple). b) The measured energy output per cycle of Mode-1/Mode-2 OA-TENG (blue/red). c) The long-term voltage output of CEO, CMEO and Mode-2 OA-TENG. d) A photograph demonstrates the illuminance of an LED under the operation of CEO, CMEO, and Mode-1 OA-TENG.

and Mode-2 OA-TENG with external load of 1 GΩ. The OA-TENG shows obvious advantage toward CEO and CMEO. We also demonstrated the advantage of OA-TENG by using a light-emitting diode (LED) as the load, as shown in Figure 5d. The LED with Mode-1 TENG is significantly brighter than that with CEO and CMEO.

4. Conclusion

We have developed a power management strategy to boost the performance of TENG. Benefited from the LC oscillation occurred at each maximum point of the displacement, the voltage and transferred charges can be accumulated and beyond the limit of CMEO. In addition to the theoretical derivation and model simulation, the performance of the OA-TENG is also experimentally demonstrated by using a mechanical switching system and a free-standing TENG. A significant energy improvement is observed compared with CEO and CMEO operations, especially for the low resistance (<1 MΩ) and ultrahigh resistance (>10 GΩ) regions. Nonideal factors in the switching system which cause the energy output lower than the theory are also discussed, accompanied with the perspectives for the future improvement. It is believed such a general, low-cost and highly effective power management strategy will soon be applied to various TENG devices and promote the industrialization and commercialization of TENG.

5. Experimental Section

Fabrication of Free-Standing Mode TENG: Typically, an acrylic sheet (thickness of 3 mm) was cut into 45 mm × 80 mm by laser cutter as the substrate. Then aluminum film (thickness of 50 μm) was stuck on the substrate before cutting an interval gap of 2 mm in the middle for forming two electrodes. A 25 μm FEP film with adhesive back was then covered on the as-fabricated electrode part to act as negative tribolayer. The sliding part of the TENG consisted of a positive nylon tribofilm (25 μm) attached rubber sponge and an acrylic sheet with the dimension of 40 mm × 35 mm. In order to form the motion triggered system, a conductive strip (width: 5 mm, length: 60 mm, thickness: 3 mm) was fixed in the middle of the slider.

Establishing the Motion Induced Trigger System: The motion triggered system consists of the TENG, oscillation electric circuit and electric brush. Firstly, several electrode nodes marked as “A,” “B,” and “C” as depicted in Figures S1 and S2 in the Supporting Information were prepared using copper tape. Then “A,” “B,” and “A,” “C” electrode nodes were fixed on two 3D stages respectively with rubber sponge using in between. The TENG part was fixed on a lifting stage and the sliding part was driven by precisely controlled linear motor. In the following, two 3D stages with electrode nodes were carefully adjusted on two sides of the conductive strip so that to ensure the connection of nodes “A,” “B” and “A,” “C” in two maximum positions. Finally, the oscillation electric circuit (Figures S1 and S2, Supporting Information) was connected between nodes “B,” “C” and electrode of TENG.

Electric Measurement Equipment: The output voltage signals and charge transfer were captured using Keithley 6514 System Electrometers. The functional motion was produced by Linear motor system (Linmot Linear guide H01-37 × 166/180).

Supporting Information

Supporting Information is available from the Wiley Online Library or from the author.

Acknowledgements

S.X., W.D., and H.G. contributed equally to this work. This research was supported by the National Natural Science Foundation of China (Grant Nos. 61834003 and 61531166006), the 973 Program of China (Grant No. 2015CB352106), and the Hightower Chair foundation. S.X. thanks China Scholarship Council for supplying oversea scholarship (201806210286).

Conflict of Interest

The authors declare no conflict of interest.

Keywords

circuit oscillation, power management, triboelectric nanogenerators

Received: March 8, 2019

Revised: June 6, 2019

Published online:

-
- [1] W. Ding, A. C. Wang, C. Wu, H. Guo, Z. L. Wang, *Adv. Mater. Technol.* **2018**, *4*, 1800487.
- [2] H. Guo, X. Pu, J. Chen, Y. Meng, M.-H. Yeh, G. Liu, Q. Tang, B. Chen, D. Liu, S. Qi, C. Wu, C. Hu, J. Wang, Z. L. Wang, *Sci. Rob.* **2018**, *3*, eaat2516.
- [3] X. Pu, H. Guo, J. Chen, X. Wang, Y. Xi, C. Hu, Z. L. Wang, *Sci. Adv.* **2017**, *3*, e1700694.
- [4] Z. L. Wang, *ACS Nano* **2013**, *7*, 9533.
- [5] Z. L. Wang, J. Chen, L. Lin, *Energy Environ. Sci.* **2015**, *8*, 2250.
- [6] Z. L. Wang, *Mater. Today* **2017**, *20*, 74.
- [7] C. Wu, A. C. Wang, W. Ding, H. Guo, Z. L. Wang, *Adv. Energy Mater.* **2019**, *9*, 1802906.
- [8] H. Guo, M.-H. Yeh, Y. Zi, Z. Wen, J. Chen, G. Liu, C. Hu, Z. L. Wang, *ACS Nano* **2017**, *11*, 4475.
- [9] J. Chen, H. Guo, X. Pu, X. Wang, Y. Xi, C. Hu, *Nano Energy* **2018**, *50*, 536.
- [10] Z. L. Wang, *Nano Energy* **2018**, *54*, 477.
- [11] F. R. Fan, Z. Q. Tian, Z. L. Wang, *Nano Energy* **2012**, *1*, 328.
- [12] C. Xu, A. C. Wang, H. Zou, B. Zhang, C. Zhang, Y. Zi, L. Pan, P. Wang, P. Feng, Z. Lin, *Adv. Mater.* **2018**, *30*, 1803968.
- [13] C. Xu, Y. Zi, A. C. Wang, H. Zou, Y. Dai, X. He, P. Wang, Y. C. Wang, P. Feng, D. Li, *Adv. Mater.* **2018**, *30*, 1706790.
- [14] J. Wang, S. Li, F. Yi, Y. Zi, J. Lin, X. Wang, Y. Xu, Z. L. Wang, *Nat. Commun.* **2016**, *7*, 12744.
- [15] J. Wang, C. Wu, Y. Dai, Z. Zhao, A. Wang, T. Zhang, Z. L. Wang, *Nat. Commun.* **2018**, *8*, 88.
- [16] F. Yi, X. Wang, S. Niu, S. Li, Y. Yin, K. Dai, G. Zhang, L. Lin, Z. Wen, H. Guo, *Sci. Adv.* **2016**, *2*, e1501624.
- [17] K. Dong, J. Deng, Y. Zi, Y. C. Wang, C. Xu, H. Zou, W. Ding, Y. Dai, B. Gu, B. Sun, *Adv. Mater.* **2017**, *29*, 1702648.
- [18] J. Peng, S. D. Kang, G. J. Snyder, *Sci. Adv.* **2017**, *3*, eaap8576.
- [19] S. Niu, S. Wang, Y. Liu, Y. S. Zhou, L. Lin, Y. Hu, K. C. Pradel, Z. L. Wang, *Energy Environ. Sci.* **2014**, *7*, 2339.
- [20] S. Niu, Y. Liu, S. Wang, L. Lin, Y. S. Zhou, Y. Hu, Z. L. Wang, *Adv. Funct. Mater.* **2014**, *24*, 3332.
- [21] S. Niu, Y. Liu, S. Wang, L. Lin, Y. S. Zhou, Y. Hu, Z. L. Wang, *Adv. Mater.* **2013**, *25*, 6184.
- [22] S. Niu, Y. Liu, Y. S. Zhou, S. Wang, L. Lin, Z. L. Wang, *IEEE Trans. Electron Devices* **2015**, *62*, 641.
- [23] Y. Zi, S. Niu, J. Wang, Z. Wen, W. Tang, Z. L. Wang, *Nat. Commun.* **2015**, *6*, 8376.
- [24] S. Niu, X. Wang, F. Yi, Y. S. Zhou, Z. L. Wang, *Nat. Commun.* **2015**, *6*, 8975.
- [25] Y. Zi, J. Wang, S. Wang, S. Li, Z. Wen, H. Guo, Z. L. Wang, *Nat. Commun.* **2016**, *7*, 10987.
- [26] A. Ghaffarinejad, J. Y. Hasani, R. Hinchet, Y. Lu, H. Zhang, A. Karami, D. Galayko, S.-W. Kim, P. Basset, *Nano Energy* **2018**, *51*, 173.
- [27] J. Shao, T. Jiang, W. Tang, X. Chen, L. Xu, Z. L. Wang, *Nano Energy* **2018**, *51*, 688.
- [28] Y. Zi, H. Guo, J. Wang, Z. Wen, S. Li, C. Hu, Z. L. Wang, *Nano Energy* **2017**, *31*, 302.
- [29] F. Xi, Y. Pang, W. Li, T. Jiang, L. Zhang, T. Guo, G. Liu, C. Zhang, Z. L. Wang, *Nano Energy* **2017**, *37*, 168.
- [30] X. Cheng, L. Miao, Y. Song, Z. Su, H. Chen, X. Chen, J. Zhang, H. Zhang, *Nano Energy* **2017**, *38*, 438.
- [31] H. Qin, G. Cheng, Y. Zi, G. Gu, B. Zhang, W. Shang, F. Yang, J. Yang, Z. Du, Z. L. Wang, *Adv. Funct. Mater.* **2018**, *28*, 1805216.
- [32] P. Brandl, R. Enne, T. Jukić, H. Zimmermann, *IEEE Photonics Technol. Lett.* **2015**, *27*, 482.
- [33] S. Niu, Y. S. Zhou, S. Wang, Y. Liu, L. Lin, Y. Bando, Z. L. Wang, *Nano Energy* **2014**, *8*, 150.
- [34] S. Niu, S. Wang, L. Lin, Y. Liu, Y. S. Zhou, Y. Hu, Z. L. Wang, *Energy Environ. Sci.* **2013**, *6*, 3576.
- [35] W. Yin, Y. Xie, J. Long, P. Zhao, J. Chen, J. Luo, X. Wang, S. Dong, *Nano Energy* **2018**, *50*, 16.
- [36] S. Niu, Z. L. Wang, *Nano Energy* **2015**, *14*, 161.
- [37] S. Niu, Y. Liu, X. Chen, S. Wang, Y. S. Zhou, L. Lin, Y. Xie, Z. L. Wang, *Nano Energy* **2015**, *12*, 760.